

Radiative Effects of Water Clouds on Heat, Cloud Microphysical and Surface Rainfall Budgets Associated with Pre-Summer Torrential Rainfall

Jia Liu¹, Xinyong Shen¹, and Xiaofan Li^{2,*}

¹Key Laboratory of Meteorological Disaster of Ministry of Education, Nanjing University of Information Science and Technology, Nanjing, China

²Department of Earth Sciences, Zhejiang University, Hangzhou, Zhejiang, China

Received 6 March 2013, accepted 2 August 2013

ABSTRACT

This study investigates thermal, cloud microphysical and surface-rainfall responses to the radiative effects of water clouds by analyzing two pairs of two-dimensional cloud-resolving model sensitivity experiments of a pre-summer heavy rainfall event. In the presence of the radiative effects of ice clouds, exclusion of the radiative effects of water clouds reduces the model domain mean rain rate through the mean hydrometeor increase, which is associated with the decreases in the melting of graupel and cloud ice caused by enhanced local atmospheric cooling. In the absence of the radiative effects of ice clouds, removal of the radiative effects of water clouds increases model domain mean rain rate via the enhancements in the mean net condensation and the mean hydrometeor loss. The enhanced mean net condensation and increased mean latent heat are related to the strengthened mean infrared radiative cooling in the lower troposphere. The increased mean hydrometeor loss associated with the reduction in the melting of graupel is caused by the enhanced local atmospheric cooling.

Key words: Radiative effects of water and ice clouds, Heat budget, Cloud microphysical budget, Surface rainfall budget

Citation: Liu, J., X. Shen, and X. Li, 2014: Radiative effects of water clouds on heat, cloud microphysical and surface rainfall budgets associated with pre-summer torrential rainfall. *Terr. Atmos. Ocean. Sci.*, 25, 39-48, doi: 10.3319/TAO.2013.08.02.01(A)

1. INTRODUCTION

Cloud radiative processes play an important role in the development of precipitation systems. The cloud-radiation interaction could lead to the destabilization of the environment (e.g., Dudhia 1989), the unstable thermal stratification of stratiform clouds in the upper troposphere (e.g., Lilly 1988), and the development of second circulation by the different radiative heating between cloudy and clear-sky regions (e.g., Gray and Jacobson 1977). Tao et al. (1993) found that infrared radiative cooling enhances surface rainfall in their cloud-resolving model simulations of precipitation systems in the tropics and mid-latitudes. Fu et al. (1995) revealed that clear-sky infrared radiative cooling enhanced rainfall while weakened infrared radiative cooling due to stratiform clouds reduces rainfall. The nocturnal rainfall peaks in the diurnal variations of surface rainfall result from the decreased saturation mixing ratio due to the falling temperature caused by the infrared radiative cooling (e.g.,

Sui et al. 1997, 1998; Gao and Li 2010).

Wang et al. (2010) and Shen et al. (2011a, b) studied cloud radiative effects of pre-summer heavy rainfall processes and found that the rainfall responses to cloud radiative processes depend on cloud type and stage of convective development. The exclusion of cloud radiative effects increases the mean rainfall during the onset and decay phases, but it reduces the mean rainfall during the mature phase (Shen et al. 2011b). The removal of the radiative effects of ice clouds reduces the mean rainfall during the onset phase, whereas it enhances the mean rainfall during the mature and decay phases. The elimination of the radiative effects of water clouds weakens the mean rainfall during the mature phase, but increases the mean rainfall during the decay phase (Shen et al. 2011a). Although Shen et al. (2011a) examined the radiative effects of water clouds on rainfall through the analysis of vertical structures of heat budget, they did not provide explanations of why and how the radiative processes of water clouds affect hydrometeor change/convergence, which may be an important rainfall generating process.

* Corresponding author
E-mail: xiaofanli@zju.edu.cn

In this study, the radiative effects of water clouds on heat, cloud microphysical and surface rainfall budgets associated with pre-summer torrential rainfall event are investigated by revisiting the sensitivity simulation data from Shen et al. (2011a). Five-day mean analysis is conducted to examine the radiative effects of water clouds on a pre-summer heavy rainfall event during 3 - 8 June 2008. Since ice clouds may reduce the incoming solar radiative flux that reaches water clouds and the outgoing infrared radiative flux emitted from water clouds and surface, the radiative processes of ice clouds may alter the radiative effects of water clouds on rainfall. Thus, the radiative effects of water clouds on heat, cloud microphysical and surface rainfall budgets will be respectively discussed in the presence and absence of the radiative effects of ice clouds. Section 2 briefly describes model, large-scale forcing, and sensitivity experiments. Section 3 discusses the analysis, and section 4 summarizes the findings.

2. MODEL AND EXPERIMENTS

The data used in this study come from Shen et al. (2011a), which are obtained from the four sensitivity experiments with a two-dimensional cloud-resolving model. Model setups used in this study are summarized in Table 1, and model microphysical schemes can be seen in Table 2. A longitudinally oriented rectangular area of 108 - 116°E, 21 - 22°N, within which torrential rainfall occurred, is chosen as the model domain for the calculation of large-scale forcing Fig. 1. The model is integrated from 0200 Local Standard Time (LST) 3 June to 0200 LST 8 June 2008, during the pre-summer heavy rainfall event. Model simulations in the control experiment (CTL) are compared with available observations in terms of rain rate, and temperature and water vapor profiles (Wang et al. 2010; Shen et al. 2011b), which show good agreement. The three sensitivity experiments are identical to the control experiment, except that the mixing

ratios of water clouds, ice clouds, and both water and ice clouds are set to zero in the calculations of radiation, in the sensitivity experiments NWR, NIR, and NCR respectively. The comparison between CTL and NWR is conducted to study the radiative effects of water clouds on rainfall in the presence of radiative effects of ice clouds. NIR and NCR are compared to examine the radiative effects of water clouds on rainfall in the absence of radiative effects of ice clouds.

3. RESULTS

3.1 Radiative Effects of Water Clouds in the Presence of Radiative Effects of Ice Clouds

In the presence of radiative effects of ice clouds, the exclusion of radiative effects of water clouds reduces the mean rain rate from 1.36 mm h⁻¹ in CTL to 1.32 mm h⁻¹ in NWR (Table 3). The mass-integrated cloud budget shows that the rain rate (P_S) is associated with the net condensation (Q_{NC}) and hydrometeor change/convergence (Q_{CM}), i.e.,

$$P_S = Q_{NC} + Q_{CM} \quad (1)$$

where

$$Q_{NC} = [P_{CND}] + [P_{DEP}] + [P_{SDEP}] + [P_{GDEF}] - ([P_{REVP}] + [P_{MLTS}] + [P_{MLTG}]) \quad (1a)$$

$$Q_{CM} = -\frac{\partial[q_s]}{\partial t} - \left[\frac{\partial}{\partial x}(uq_s)\right] \quad (1b)$$

$q_s = q_c + q_r + q_i + q_s + q_g$, q_c , q_r , q_i , q_s , and q_g are the mixing ratios of cloud water, raindrops, cloud ice, snow, and graupel, respectively; $[\] = \int_{z_b}^{z_t} \bar{\rho} dz$, z_t and z_b are the heights of the top and bottom of the model atmosphere respectively;

Table 1. Model setups.

Model history	The model was originally developed by Soong and Ogura (1980), Soong and Tao (1980), and Tao and Simpson (1993) and was further modified by Sui et al. (1994, 1998) and Li et al. (1999, 2002).
Prognostic equations	Potential temperature, specific humidity, five hydrometeor species, and perturbation zonal wind and vertical velocity.
Cloud microphysical schemes	Lin et al. (1983); Rutledge and Hobbs (1983, 1984); Tao et al. (1989); and Krueger et al. (1995), also Table 2.
Radiation schemes	Chou et al. (1998); Chou et al. (1991); Chou and Suarez (1994).
Basic model parameters	Model domain of 768 km, grid mesh of 1.5 km, time step of 12 s, and 33 vertical layers.
Lateral boundary conditions	Cyclic
Model reference	Gao and Li (2008) and Li and Gao (2011)
Model integration	0200 LST 3 June - 0200 LST 8 June 2008
Large-scale forcing	Vertical velocity and zonal wind (see Fig. 1), and horizontal advectons (not shown).
Model surface boundary conditions	The surface temperature and specific humidity from NCEP/GDAS are also imposed in the model to calculate surface sensible heat flux and evaporation flux.

Table 2. List of microphysical processes and their parameterization schemes [Lin et al. (1983, LFO), Rutledge and Hobbs (1983; 1984; RH83, RH84), Tao et al. (1989, TSM), and Krueger et al. (1995, KFLC)].

Notation	Description	Scheme
P_{MLTG}	Growth of vapor by evaporation of liquid from graupel surface	RH84
P_{MLTS}	Growth of vapor by evaporation of melting snow	RH83
P_{REVP}	Growth of vapor by evaporation of raindrops	RH83
P_{IMLT}	Growth of cloud water by melting of cloud ice	RH83
P_{CND}	Growth of cloud water by condensation of supersaturated vapor	TSM
P_{GMLT}	Growth of raindrops by melting of graupel	RH84
P_{SMLT}	Growth of raindrops by melting of snow	RH83
P_{RACI}	Growth of raindrops by the accretion of cloud ice	RH84
P_{RACW}	Growth of raindrops by the collection of cloud water	RH83
P_{RACS}	Growth of raindrops by the accretion of snow	RH84
P_{RAUT}	Growth of raindrops by the autoconversion of cloud water	LFO
P_{IDW}	Growth of cloud ice by the deposition of cloud water	KFLC
P_{IACR}	Growth of cloud ice by the accretion of rain	RH84
P_{IHOM}	Growth of cloud ice by the homogeneous freezing of cloud water	
P_{DEP}	Growth of cloud ice by the deposition of supersaturated vapor	TSM
P_{SAUT}	Growth of snow by the conversion of cloud ice	RH83
P_{SACI}	Growth of snow by the collection of cloud ice	RH83
P_{SACW}	Growth of snow by the accretion of cloud water	RH83
P_{SEW}	Growth of snow by the deposition of cloud water	KFLC
P_{SFI}	Depositional growth of snow from cloud ice	KFLC
P_{SACR}	Growth of snow by the accretion of raindrops	LFO
P_{SDEP}	Growth of snow by the deposition of vapor	RH83
P_{GACI}	Growth of graupel by the collection of cloud ice	RH84
P_{GACR}	Growth of graupel by the accretion of raindrops	RH84
P_{GACS}	Growth of graupel by the accretion of snow	RH84
P_{GACW}	Growth of graupel by the accretion of cloud water	RH84
P_{WACS}	Growth of graupel by the riming of snow	RH84
P_{GDEP}	Growth of graupel by the deposition of vapor	RH84
P_{GFR}	Growth of graupel by the freezing of raindrops	LFO

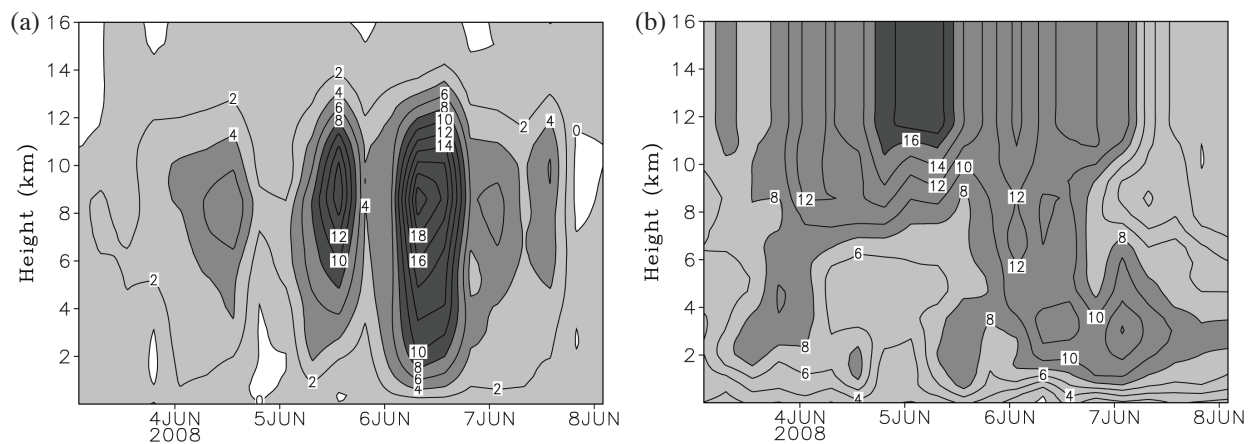


Fig. 1. Temporal and vertical distribution of (a) vertical velocity (cm s^{-1}) and (b) zonal wind (m s^{-1}) from 0200 LST 3 June - 0200 LST 8 June 2008. The data are averaged in a rectangular box of $108 - 116^\circ\text{E}$, $21 - 22^\circ\text{N}$ from NCEP/GDAS data. Ascending motion in (a) and westerly wind in (b) are shaded.

Table 3. Cloud microphysical budgets (P_S , Q_{NC} , and Q_{CM}) averaged for 5 days over the model domain in CTL, NWR, NIR, and NCR, and their differences between NWR and CTL (NWR-CTL) and NCR and NIR (NCR-NIR). Unit is mm h^{-1} .

	CTL	NWR	NIR	NCR	NWR-CTL	NCR-NIR
P_S	1.364	1.322	1.326	1.358	-0.042	0.032
Q_{NC}	1.333	1.347	1.326	1.344	0.014	0.018
Q_{CM}	0.031	-0.025	0.0	0.014	-0.056	0.014

$([P_{CND}] + [P_{DEP}] + [P_{SDEP}] + [P_{GDEP}])$ represents the cloud source term that consists of vapor condensation rate for the growth of cloud water ($[P_{CND}]$), vapor deposition rates for the growth of cloud ice ($[P_{DEP}]$), snow ($[P_{SDEP}]$) and graupel ($[P_{GDEP}]$); $-([P_{REVP}] + [P_{MLTG}] + [P_{MLTS}])$ denotes the cloud sink term that includes growth of vapor by evaporation of raindrops ($[P_{REVP}]$), evaporation of liquid from graupel surfaces ($[P_{MLTG}]$), and evaporation of melting snow ($[P_{MLTS}]$). Comparison of the mean cloud microphysical budget between CTL and NWR reveals that the weakened mean rain rate from CTL to NWR is associated with the mean hydrometeor change from a loss in CTL to a gain in NWR while the mean net condensation increases from CTL to NWR. Note that the model domain mean hydrometeor convergence is zero due to the cyclic lateral boundaries furnished in the model. Since the radiative effects of ice clouds are the term in the heat budget, the mean heat budget can be analyzed. Following Li et al. (1999), the model domain mean heat and specific humidity budgets can be expressed by

$$\begin{aligned} \frac{\partial \bar{T}}{\partial t} = & \frac{\bar{Q}_{cn}}{c_p} + \frac{\bar{Q}_R}{c_p} - \frac{\pi}{\rho} \frac{\partial (\bar{\rho} \bar{w}' \bar{\theta}')}{\partial z} \\ & - \pi \bar{w}' \frac{\partial \bar{\theta}}{\partial z} - \bar{u}' \frac{\partial \bar{T}}{\partial x} \end{aligned} \quad (2)$$

Here, $\pi = (p / p_o)^\kappa$ and $\kappa = R / c_p$; R is the gas constant; c_p is the specific heat of dry air at constant pressure p , and $p_o = 1000$ mb; ρ is height-dependent air density; T is the air temperature, θ is the potential temperature; u and w are the zonal and vertical components of winds; Q_{cn} is the latent heat due to the phase change between water vapor and five cloud species; Q_R is the radiative heating rate due to convergence of the net flux of solar and infrared radiative fluxes; overbar denotes model domain mean, and prime is perturbation from the domain mean; subscript "o" is a value imposed on the model, which is constructed from National Centers for Environmental Prediction/Global Data Assimilation System (NCEP/GDAS) The heat budget (2) states that the local change of model domain mean temperature is determined by condensational heating, radiative heating, convergence of vertical heat flux, vertical temperature advection, and imposed horizontal temperature advection.

The removal of the radiative effects of water clouds weakens the mean infrared radiative cooling from CTL to NWR from altitudes of 2 to 13 km (Fig. 2b). The reduced mean latent heat between altitudes of 2.5 and 6.5 km corresponds to the weakened mean infrared radiative cooling (Fig. 2a). The suppressed mean latent heat tends to cool the local atmosphere at altitudes between 2.5 and 4.5 km, which causes an unstable vertical stratification near the surface.

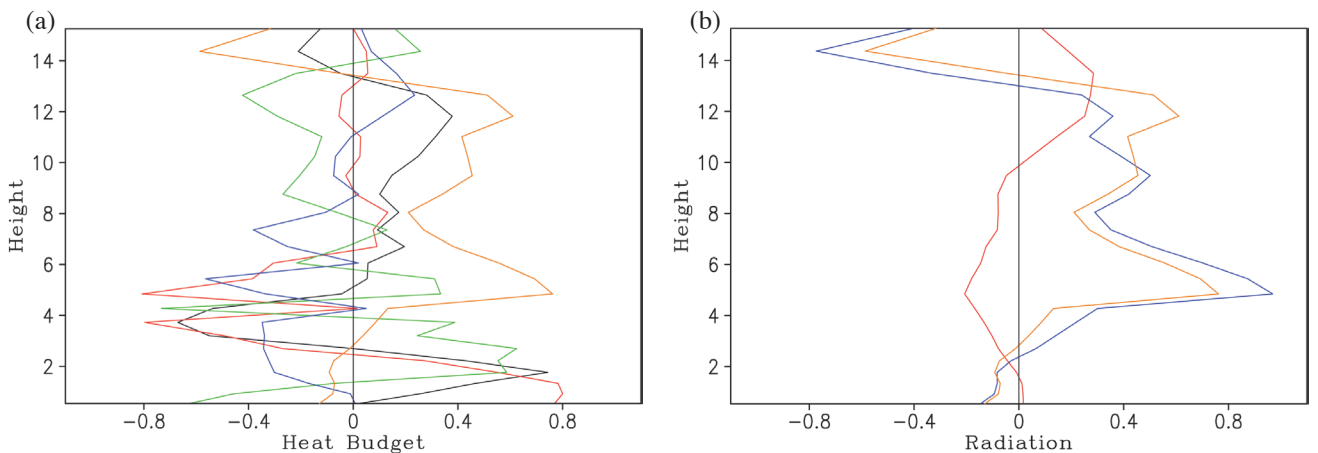


Fig. 2. Vertical profiles of differences between NWR and CTL (NWR-CTL) for (a) local temperature changes (black), latent heat (red), convergence of vertical heat flux (green), vertical temperature advection (blue), and radiation (orange), and (b) radiation (orange) and its solar heating (red) and infrared cooling (blue) components averaged for 5 days and model domain. Unit is $^{\circ}\text{C d}^{-1}$.

In addition, the reduced net condensation associated with the decreased mean latent heat decreases the consumption of water vapor, which is available for the enhancement of convection near the surface. As a result, the mean net condensation and associated mean latent heat increase near the surface. The enhanced mean latent heat near the surface is largely canceled by the weakened mean latent heat in the mid troposphere, but the magnitude of the former is larger than that of the latter, which leads to a slight increase in the mean net condensation from CTL to NWR (Table 3).

To examine the difference in Q_{CM} between CTL and NWR, the mean cloud microphysical budgets are analyzed. Q_{CM} can be broken down to

$$Q_{CMC} = -\frac{\partial[q_c]}{\partial t} - \left[\frac{\partial}{\partial x}(uq_c)\right] = -Sq_c \quad (3a)$$

$$Q_{CMR} = -\frac{\partial[q_r]}{\partial t} - \left[\frac{\partial}{\partial x}(uq_r)\right] = -Sqr + P_s \quad (3b)$$

$$Q_{CMI} = -\frac{\partial[q_i]}{\partial t} - \left[\frac{\partial}{\partial x}(uq_i)\right] = -Sqi \quad (3c)$$

$$Q_{CMS} = -\frac{\partial[q_s]}{\partial t} - \left[\frac{\partial}{\partial x}(uq_s)\right] = -Sqs \quad (3d)$$

$$Q_{CMG} = -\frac{\partial[q_g]}{\partial t} - \left[\frac{\partial}{\partial x}(uq_g)\right] = -Sqg \quad (3e)$$

The comparison in the mean cloud microphysical budget between CTL and NWR reveals similar Q_{CMR} (-0.01 mm h^{-1}) in the two experiments (Fig. 3). The difference in Q_{CM} is associated with the differences in Q_{CMC} (0.0 in CTL versus -0.02 mm h^{-1} in NWR), Q_{CMI} (0.02 mm h^{-1} in CTL versus 0.0 in NWR), and Q_{CMG} (0.02 mm h^{-1} in CTL versus 0.0 in NWR). The vapor condensation rate (P_{CND}) is larger in NWR than in CTL forming a source for cloud water in NWR, while the collection rate of cloud water by rain (P_{RACW}) and the accretion rate of cloud water by graupel [$P_{GACW}(T < T_0)$] are larger in CTL than in NWR as a result of the melting of cloud ice to cloud water (P_{IMLT}). Compared to those in CTL, more vapor condensation in NWR may be related to more water vapor due to less consumption of water vapor as indicated by less rainfall. Compared to those in NWR, the melting of cloud ice to cloud water is the microphysical process that is responsible for the sink for cloud ice in CTL. The melting of graupel to rain (P_{GMLT}) is larger in CTL than in NWR, which leads to a sink for graupel in CTL. The melting of cloud ice to cloud water in CTL and the enhancement in the melting of graupel to rain from NWR to CTL may be associated with the reduced atmospheric cooling from 2.5 to 4.5 km, which corresponds to the increased convergence

of vertical heat flux from NWR to CTL at altitudes around 4 km and the suppressed heat divergence and enhanced latent heat NWR to CTL between 2.5 and 4 km (Fig. 2a).

The reduction in mean rain rate caused by the exclusion of the radiative effects of water clouds can also be examined by analyzing surface rainfall budget. In the surface rainfall budget (Gao et al. 2005; Cui and Li 2006), the rain rate is associated with local water-vapor change (Q_{WVT}), water vapor convergence (Q_{WVF}), surface evaporation (Q_{WVE}), and hydrometeor change/convergence (Q_{CM}), i.e.,

$$P_s = Q_{WVT} + Q_{WVF} + Q_{WVE} + Q_{CM} \quad (4)$$

where

$$Q_{WVT} = -\frac{\partial[q_v]}{\partial t} \quad (4a)$$

$$Q_{WVF} = -[\bar{u}^\circ \frac{\partial \bar{q}_v^\circ}{\partial x}] - [\frac{\partial}{\partial x}(\bar{u}^\circ + u')q_v'] - [\bar{w}^\circ \frac{\partial \bar{q}_v^\circ}{\partial z}] - [\bar{w}'^\circ \frac{\partial q_v'}{\partial z}] - [w' \frac{\partial \bar{q}_v^\circ}{\partial z}] \quad (4b)$$

$$Q_{WVE} = E_s \quad (4c)$$

q_v is the specific humidity; u and w are the zonal and vertical components of wind, respectively; E_s is the surface evaporation rate; overbar denotes a spatial mean; prime is a perturbation from spatial mean, and the superscript $^\circ$ defines imposed NCEP/GDAS data.

Shen et al. (2010) analyzed grid-scale simulation data of tropical rainfall by partitioning them into eight rainfall types based on the surface rainfall budget. Shen et al. (2012) applied this rainfall separation scheme to the evaluation of an existing convective-stratiform rainfall separation scheme based on the rain intensity (e.g., Tao et al. 1993) and found that the convective rainfall contains a considerable amount of rainfall associated with water vapor divergence. Since convective and stratiform rainfalls are associated with water vapor convergence and divergence, respectively, we separated the grid-scale rainfall simulation data into rain types associated with water vapor convergence and divergence. Table 4 reveals that the reduction in the mean rain rate from CTL to NWR results from the weakened rain rate associated with water vapor divergence, which corresponds to the slowdown in hydrometeor loss/convergence while the reduced water vapor divergence decreases local atmospheric drying.

3.2 Radiative Effects of Water Clouds in the Absence of Radiative Effects of Ice Clouds

In the absence of the radiative effects of ice clouds,

exclusion of the radiative effects of water clouds increases the mean rain rate through the increased mean net condensation from NIR to NCR and the mean hydrometeor loss in NCR (Table 3). A comparison of the mean heat budget between the two experiments shows that the removal of radiative effects of water clouds weakens the mean infrared radiative cooling and the mean solar radiative heating at altitudes above 4.5 and 3 km respectively, but enhances the mean infrared radiative cooling and increases the mean solar radiative heating at altitudes below 4 and 3 km, respectively (Fig. 4). As a result, the suppressed mean latent heat above 3.5 km altitude corresponds to the weakened mean infrared radiative cooling, whereas the enhanced mean latent heat below 3.5 km corresponds to the strengthened mean infrared radiative cooling (Fig. 4a). The weakened mean latent heat in the mid and upper troposphere is largely offset by the intensified mean latent heat in the lower troposphere, which causes a slight increase in the net condensation in a mass integration from NIR to NCR. The analysis of cloud microphysical budgets shown in Fig. 5 reveals that the difference in Q_{CM} is associated with the differences in Q_{CMR} (0.01 mm h^{-1} in NIR versus 0.02 mm h^{-1} in NCR), Q_{CMS} (-0.01 mm h^{-1} in NIR versus 0.0 in NCR), and Q_{CMG} (0.01 mm h^{-1} in NIR versus 0.0 in NCR) (Fig. 5). Q_{CMR} is slightly larger in NCR than NIR because the melting rate of graupel to rain is slightly lower in NCR than NIR. The reduction in the melting from NIR to NCR may be associated with enhanced local atmospheric cooling above 4 km (Fig. 4a), which is caused by the suppressed mean latent heat and weakened convergence of vertical heat flux. $Q_{CMS} + Q_{CMG} = 0$ in NIR mainly due to the fact the accretion rate of snow by graupel (P_{GACS}) is slightly lower in NIR than NCR.

The enhanced rainfall from NIR to NCR is caused by the increased rainfall associated with water vapor divergence, which is associated with the strengthened hydrome-

teor loss/convergence while the intensified water vapor divergence increases the local atmospheric drying.

4. SUMMARY

The radiative effects of water clouds on heat, cloud microphysical and surface rainfall budgets during pre-summer rainfall over southern China were examined through the analysis of sensitivity experiment data for a heavy rainfall event that occurred from 3 - 8 June 2008. The control experiment and sensitivity experiment without the radiative effects of water clouds were compared to study the rainfall responses to the radiative effects of water clouds when the radiative effects of ice clouds were turned on. The sensitivity experiments without the radiative effects of ice clouds and cloud-radiation interaction were also compared to study the rainfall responses to water cloud-radiation interaction when the radiative effects of ice clouds were turned off. The main conclusions are:

- (1) In the presence of the radiative effects of ice clouds, exclusion of the radiative effects of water clouds reduces the model domain mean rain rate through the mean hydrometeor change from a loss in the control experiment (CTL) to a gain in the sensitivity experiment without radiative effects of water clouds (NWR). Such a mean hydrometeor change results from decreases in the melting of graupel and cloud ice from CTL to NWR due to enhanced atmospheric cooling.
- (2) In the absence of the radiative effects of ice clouds, removal of the radiative effects of water clouds increases model-domain mean rain rate via enhancements in the mean net condensation and the mean hydrometeor loss. The enhanced mean net condensation is associated with the increased mean latent heat, which corresponds to the strengthened mean infrared radiative cooling in the lower

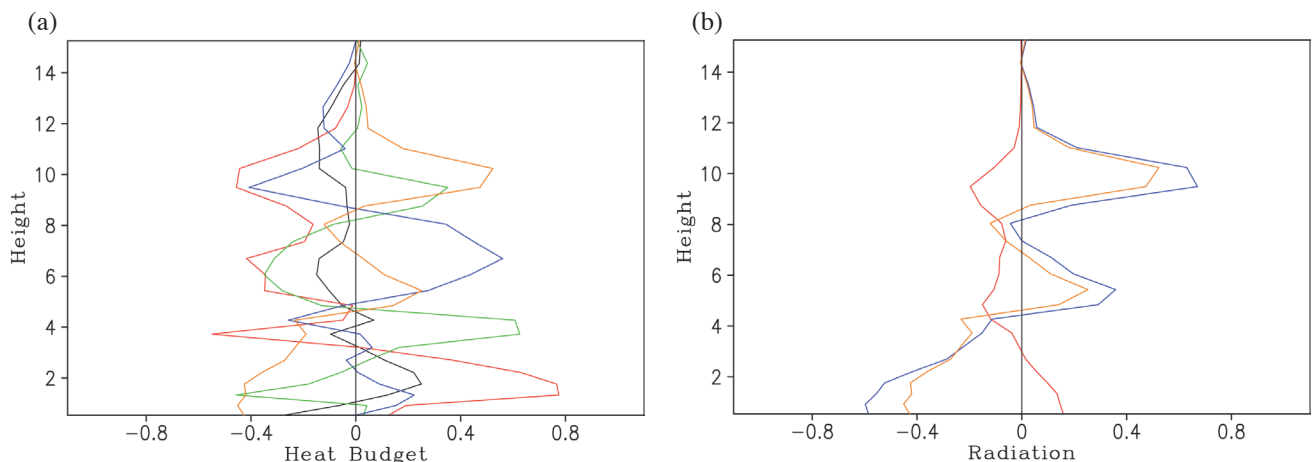


Fig. 4. Vertical profiles of differences between NCR and NIR (NCR - NIR) for (a) local temperature changes (black), latent heat (red), convergence of vertical heat flux (green), vertical temperature advection (blue), and radiation (orange), and (b) radiation (orange) and its solar heating (red) and infrared cooling (blue) components averaged for 5 days and model domain. Unit is $^{\circ}\text{C d}^{-1}$.

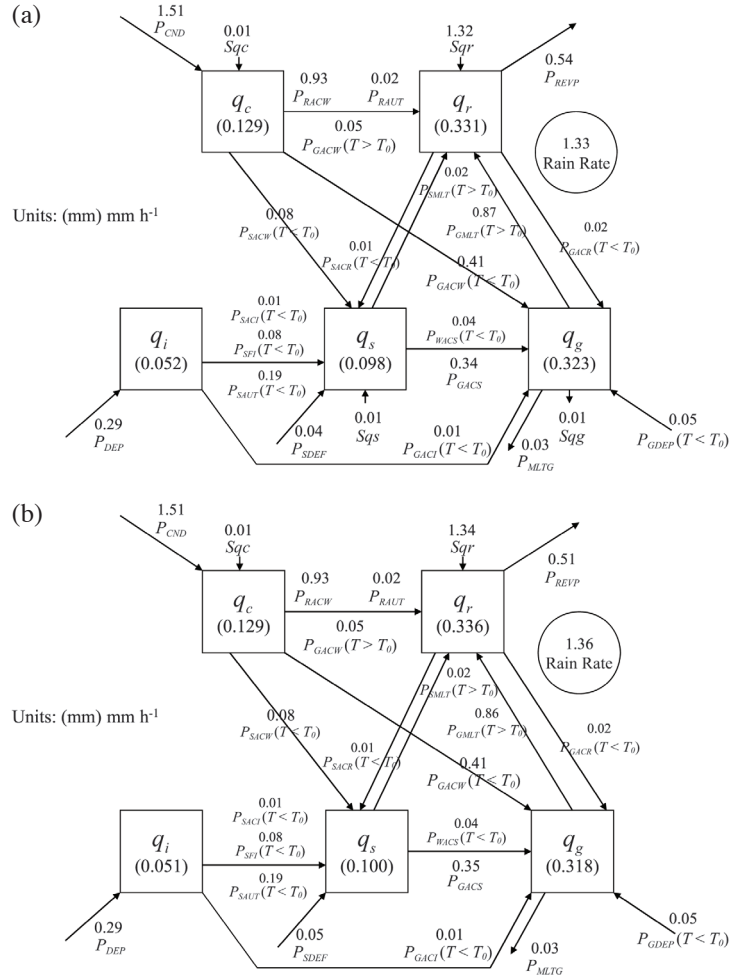


Fig. 5. Time mean cloud microphysical budgets in (a) NIR and (b) NCR. Units for cloud hydrometeors and conversions are mm and mm h⁻¹, respectively. Cloud microphysical conversion terms and their schemes can be found in Table 2. $T_0 = 0^\circ\text{C}$.

troposphere. The increased mean hydrometeor loss is related to the reduction in the melting of graupel caused by enhanced local atmospheric cooling.

- (3) An analysis of the surface rainfall budget shows that the radiative effects of water clouds have the most influence on the rain type associated with local atmospheric drying, water vapor divergence and hydrometeor convergence: the main components of stratiform rainfall. Exclusion of the radiative effects of water clouds reduces hydrometeor convergence when the radiative effects of ice clouds are included in the simulation, but strengthens hydrometeor convergence when they are removed.

Caution should be exercised in applying the results from this study, since the model is two-dimensional and driven by large-scale forcing. Three-dimensional interactive cloud-resolving model experiments are required to validate two-dimensional results of this study.

Acknowledgments The authors thank Dr. W. K. Tao (NASA/GSFC) for making his cloud-resolving model software available. Prof. C. H. Sui (National Taiwan Uni-

versity) and the anonymous reviewers also provided constructive comments that improved the early version of the manuscript. This study was supported by the National Key Basic Research and Development Project of China under Grant Nos. 2013CB430103 and 2011CB403405, the National Natural Science Foundation of China under Grant Nos. 41375058 and 41075039, the Priority Academic Program Development of Jiangsu Higher Education Institutions (PAPD), and the 985 program of Zhejiang University under Grant No 188020+193432602/215.

REFERENCES

- Chou, M. D. and M. J. Suarez, 1994: An efficient thermal infrared radiation parameterization for use in general circulation models, NASA Tech. Memo. 104606, Vol. 3, NASA/Goddard Space Flight Center, Greenbelt, 85 pp.
- Chou, M. D., D. P. Kratz, and W. Ridgway, 1991: Infrared radiation parameterizations in numerical climate models. *J. Climate*, **4**, 424-437, doi: 10.1175/1520-044

- 2(1991)004<0424:IRPINC>2.0.CO;2. [[Link](#)]
- Chou, M. D., M. J. Suarez, C. H. Ho, M. M. H. Yan, and K. T. Lee, 1998: Parameterizations for cloud overlapping and shortwave single-scattering properties for use in general circulation and cloud ensemble models. *J. Climate*, **11**, 202-214, doi: 10.1175/1520-0442(1998)011<0202:PFCOAS>2.0.CO;2. [[Link](#)]
- Cui, X. and X. Li, 2006: Role of surface evaporation in surface rainfall processes. *J. Geophys. Res.*, **111**, D17112, doi: 10.1029/2005JD006876. [[Link](#)]
- Dudhia, J., 1989: Numerical study of convection observed during the winter monsoon experiment using a mesoscale two-dimensional model. *J. Atmos. Sci.*, **46**, 3077-3107, doi: 10.1175/1520-0469(1989)046<3077:NSOCOD>2.0.CO;2. [[Link](#)]
- Fu, Q., S. K. Krueger, and K. N. Liou, 1995: Interactions of radiation and convection in simulated tropical cloud clusters. *J. Atmos. Sci.*, **52**, 1310-1328, doi: 10.1175/1520-0469(1995)052<1310:IORACI>2.0.CO;2. [[Link](#)]
- Gao, S. and X. Li, 2008: *Cloud-Resolving Modeling of Convective Processes*, Springer, Dordrecht, 206 pp.
- Gao, S. and X. Li, 2010: Precipitation equations and their applications to the analysis of diurnal variation of tropical oceanic rainfall. *J. Geophys. Res.*, **115**, D08204, doi: 10.1029/2009JD012452. [[Link](#)]
- Gao, S., X. Cui, Y. Zhou, and X. Li, 2005: Surface rainfall processes as simulated in a cloud-resolving model. *J. Geophys. Res.*, **110**, D10202, doi: 10.1029/2004JD005467. [[Link](#)]
- Gray, W. M. and R. W. Jacobson Jr., 1977: Diurnal variation of deep cumulus convection. *Mon. Weather Rev.*, **105**, 1171-1188, doi: 10.1175/1520-0493(1977)105<1171:DVODCC>2.0.CO;2. [[Link](#)]
- Krueger, S. K., Q. Fu, K. N. Liou, and H. N. S. Chin, 1995: Improvements of an ice-phase microphysics parameterization for use in numerical simulations of tropical convection. *J. Appl. Meteorol.*, **34**, 281-287, doi: 10.1175/1520-0450-34.1.281. [[Link](#)]
- Li, X. and S. Gao, 2011: *Precipitation Modeling and Quantitative Analysis*, Springer, Dordrecht, 240 pp.
- Li, X., C. H. Sui, K. M. Lau, and M. D. Chou, 1999: Large-scale forcing and cloud-radiation interaction in the tropical deep convective regime. *J. Atmos. Sci.*, **56**, 3028-3042, doi: 10.1175/1520-0469(1999)056<3028:LSFACR>2.0.CO;2. [[Link](#)]
- Li, X., C. H. Sui, and K. M. Lau, 2002: Dominant cloud microphysical processes in a tropical oceanic convective system: A 2D cloud resolving modeling study. *Mon. Weather Rev.*, **130**, 2481-2491, doi: 10.1175/1520-0493(2002)130<2481:DCMPIA>2.0.CO;2. [[Link](#)]
- Lilly, D. K., 1988: Cirrus outflow dynamics. *J. Atmos. Sci.*, **45**, 1594-1605, doi: 10.1175/1520-0469(1988)045<1594:COD>2.0.CO;2. [[Link](#)]
- Lin, Y. L., R. D. Farley, and H. D. Orville, 1983: Bulk parameterization of the snow field in a cloud model. *J. Clim. Appl. Meteorol.*, **22**, 1065-1092, doi: 10.1175/1520-0450(1983)022<1065:BPOTSF>2.0.CO;2. [[Link](#)]
- Rutledge, S. A. and P. V. Hobbs, 1983: The mesoscale and microscale structure and organization of clouds and precipitation in midlatitude cyclones. VIII: A model for the "seeder-feeder" process in warm-frontal rainbands. *J. Atmos. Sci.*, **40**, 1185-1206, doi: 10.1175/1520-0469(1983)040<1185:TMAMSA>2.0.CO;2. [[Link](#)]
- Rutledge, S. A. and P. V. Hobbs, 1984: The mesoscale and microscale structure and organization of clouds and precipitation in midlatitude cyclones. XII: A diagnostic modeling study of precipitation development in narrow cold-frontal rainbands. *J. Atmos. Sci.*, **41**, 2949-2972, doi: 10.1175/1520-0469(1984)041<2949:TMAMSA>2.0.CO;2. [[Link](#)]
- Shen, X., Y. Wang, N. Zhang, and X. Li, 2010: Precipitation and cloud statistics in the deep tropical convective regime. *J. Geophys. Res.*, **115**, D24205, doi: 10.1029/2010JD014481. [[Link](#)]
- Shen, X., Y. Wang, and X. Li, 2011a: Radiative effects of water clouds on rainfall responses to the large-scale forcing during pre-summer heavy rainfall over Southern China. *Atmos. Res.*, **99**, 120-128, doi: 10.1016/j.atmosres.2010.09.011. [[Link](#)]
- Shen, X., Y. Wang, and X. Li, 2011b: Effects of vertical wind shear and cloud radiative processes on responses of rainfall to the large-scale forcing during pre-summer heavy rainfall over southern China. *Q. J. Roy. Meteor. Soc.*, **137**, 236-249, doi: 10.1002/qj.735. [[Link](#)]
- Shen, X., J. Liu, and X. Li, 2012: Evaluation of convective-stratiform rainfall separation schemes by precipitation and cloud statistics. *J. Trop. Meteorol.*, **18**, 98-107, doi: 10.3969/j.issn.1006-8775.2012.01.011. [[Link](#)]
- Soong, S. T. and W. K. Tao, 1980: Response of deep tropical cumulus clouds to Mesoscale processes. *J. Atmos. Sci.*, **37**, 2016-2034, doi: 10.1175/1520-0469(1980)037<2016:RODTCC>2.0.CO;2. [[Link](#)]
- Soong, S. T. and Y. Ogura, 1980: Response of tradewind cumuli to large-scale processes. *J. Atmos. Sci.*, **37**, 2035-2050, doi: 10.1175/1520-0469(1980)037<2035:RODTCC>2.0.CO;2. [[Link](#)]
- Sui, C. H., K. M. Lau, W. K. Tao, and J. Simpson, 1994: The tropical water and energy cycles in a cumulus ensemble model. Part I: Equilibrium climate. *J. Atmos. Sci.*, **51**, 711-728, doi: 10.1175/1520-0469(1994)051<0711:TTWAEC>2.0.CO;2. [[Link](#)]
- Sui, C. H., K. M. Lau, Y. N. Takayabu, and D. A. Short, 1997: Diurnal variations in tropical oceanic cumulus convection during TOGA COARE. *J. Atmos. Sci.*, **54**, 639-655, doi: 10.1175/1520-0469(1997)054<0639:DVITOC>2.0.CO;2. [[Link](#)]
- Sui, C. H., X. Li, and K. M. Lau, 1998: Radiative-convective processes in simulated diurnal variations of tropical

- oceanic convection. *J. Atmos. Sci.*, **55**, 2345-2357, doi: 10.1175/1520-0469(1998)055<2345:RCPISD>2.0.CO;2. [[Link](#)]
- Tao, W. K. and J. Simpson, 1993: Goddard Cumulus Ensemble model. Part I: Model description. *Terr. Atmos. Ocean. Sci.*, **4**, 35-72.
- Tao, W. K., J. Simpson, and M. McCumber, 1989: An ice-water saturation adjustment. *Mon. Weather Rev.*, **117**, 231-235, doi: 10.1175/1520-0493(1989)117<0231:AI-WSA>2.0.CO;2. [[Link](#)]
- Tao, W. K., J. Simpson, C. H. Sui, B. Ferrier, S. Lang, J. Scala, M. D. Chou, and K. Pickering, 1993: Heating, moisture, and water budgets of tropical and midlatitude squall lines: Comparisons and sensitivity to long-wave radiation. *J. Atmos. Sci.*, **50**, 673-690, doi: 10.1175/1520-0469(1993)050<0673:HMAWBO>2.0.CO;2. [[Link](#)]
- Wang, Y., X. Shen, and X. Li, 2010: Microphysical and radiative effects of ice clouds on responses of rainfall to the large-scale forcing during pre-summer heavy rainfall over southern China. *Atmos. Res.*, **97**, 35-46, doi: 10.1016/j.atmosres.2010.03.005. [[Link](#)]